Efficient Viscosity and Thermal Conductivity Formulation for Scale-Resolved Hypersonic Flow Simulations

Ali Musawi* and Neil D. Sandham†
University of Southampton, Boldrewood Innovation Campus, Burgess Rd, Southampton SO16 7QF, U.K.

Under high enthalpy conditions, the calculation of transport properties such as viscosity and thermal conductivity needs to account for non-equilibrium effects, including vibrational non-equilibrium and the dissociation of molecules. Current models require computationally intensive mixing rules and are limited to certain temperature ranges. With scale-resolving simulation becoming more commonplace, there is a need for efficient formulations that can cover a wide range of temperatures. In this contribution, a simplified formulation is proposed for the viscosity and thermal conductivity of air in the temperature range $100K$ to $9000K$. Thermal conductivity is decomposed into ro-translational and vibrational contributions for molecular species. The predictions are applicable to both equilibrium and non-equilibrium conditions. For equilibrium air, the predictions are typically within a few percent of reference data. An application to a transitional mixing layer, starting with partially dissociated air at a temperature of $6000K$, is presented. The mixing layer is simulated with a high-order finite difference method and undergoes inflectional instability and transition to turbulence. With the new method the transport properties are within 2.2% of reference values, while the reduced complexity means that the simulations are substantially faster.

Nomenclature

$A^\star$	=	Lennard-Jones potential mixture transport property quantity
a_{av}	=	average value of non-diagonal matrix element
c_p	=	mixture specific heat at constant pressure, J/(kg · K)
c_{p_s}	=	specific heat at constant pressure for species s, J/(kg · K)
D_s	=	effective diffusion coefficient for species s, m^2/s
E	=	total energy, J/kg
e_v	=	mixture vibrational energy, J/kg

*PhD Student, Aerodynamics and Flight Mechanics Group, University of Southampton; m.a.musawi@soton.ac.uk (Corresponding Author)
†Professor of Aerospace Engineering, Aerodynamics and Flight Mechanics Group, University of Southampton; n.sandham@soton.ac.uk
Presented at the AIAA SciTech Forum, Orlando, FL, January 2025. Paper: AIAA-2025-0340

$e_{v,s}$ = vibrational energy for species s, J/kg

$e^*_{v,s}$ = equilibrium vibrational energy for species s, J/kg

ϵ/k = potential parameter, K

H = total enthalpy, J/kg

h_s = enthalpy for species s, J/kg

$h^\circ_{f_s}$ = enthalpy of formation for species s, J/kg

K = total thermal conductivity, W/(m · K)

K_c = thermal conductivity critical enhancement, W/(m · K)

K_0 = dilute gas thermal conductivity, W/(m · K)

K_r = rotational component of thermal conductivity, W/(m · K)

K_t = translational component of thermal conductivity, W/(m · K)

K_{tr} = ro-translational component of thermal conductivity, J/(m · s)

K_v = vibrational component of thermal conductivity, J/(m · s)

k = Boltzmann constant, erg/K

L_x, L_y, L_z = domain lengths in x, y and z directions respectively, m

M_s = molecular weight for species s, kg/(kg · mol)

N_A = Avogadro number, mol/(g · mol)

N_i, t_i, d_i, l_i = constants used for the Lemmon-Jacobsen model

p = mixture pressure, Pa

R_i = thermal conductivity ratio

ρ = mixture density, kg/m^3

ρ_c = critical density, kg/m^3

ρ_s = density for species s, kg/m^3

σ_{ij} = binary collision diameter, m

σ_s = collision diameter for species s, m

T = translational temperature, K

T^* = reduced temperature (kT/ϵ), K

T_c = critical temperature, K

T_v = vibrational temperature, K

T_e = electronic temperature, K

τ_s = vibrational relaxation for species s, s

u = velocity component in x direction, m/s

$u_{i,j,k}$ = velocity vector in the x, y, and z directions

v = velocity component in y direction, m/s

w = velocity component in z direction, m/s

X_s = mole fraction for species s

$\dot{\omega}_s$ = mass rate of production of species s, kg/m$^3 \cdot$ s

$\mathscr{R}$ = universal gas constant , J/(mol $\cdot$ K)

μ = mixture viscosity, kg/(m $\cdot$ s)

μ_0 = dilute gas viscosity, kg/(m $\cdot$ s)

μ_{re} = residual fluid viscosity, kg/(m $\cdot$ s)

$\delta_{i,j}$ = Kronecker delta

$\overline{\Omega}_{ij}^{(l,s)}$ = weighted average of the collision cross section between species i and j, m^2

$\Omega^{(l,s)}$ = collision cross section, m^2

I. Introduction

The hypersonic flight regime presents significant challenges for both experimental studies—due to limitations in measurement techniques and difficulties in controlling background turbulence levels—and for simulations, owing to the presence of shock waves and steep temperature gradients near surfaces. As computational power increases, scale-resolved simulations, such as direct numerical simulations (DNS) and large-eddy simulations (LES), are increasingly complementing experimental efforts and providing fundamental insights. Much of the work to date has focused on 'cold' or 'classical' hypersonic conditions, where high-temperature effects are absent, and most simulations have utilised Sutherland's law for viscosity and a constant Prandtl number to estimate thermal conductivity. However, these approximations break down under 'hot' or 'high-enthalpy' conditions, which require a more fundamental approach to gas dynamics modeling [1–4]. Current models for these conditions are complex and computationally demanding; for example, the Yos-Gupta model [5] (defined below) incorporates detailed mixing rules but is only accurate above $1000K$, which would exclude, for example, the flow near cooled walls. In this connection, a DNS/LES code would preferably not require the use of conditional statements to apply different formulations across different temperature ranges, especially when evaluating potentially billions of grid points over millions of iterations. This paper therefore aims to construct efficient models that are valid over a wide temperature range.

In strongly non-equilibrium flows, where the characteristic timescales of the flow become comparable to those of relaxation processes, it becomes necessary to couple the equations governing macroscopic parameters with those for physico-chemical kinetics. Under these conditions, transport coefficients, heat flux, and diffusion velocities are directly influenced by the non-equilibrium state [6]. Consequently, accurately capturing the effects of non-equilibrium kinetics

on transport properties and their formulation becomes crucial. By employing the distribution function as a solution to the Boltzmann equation, which provides expressions for the flux vectors, transport coefficients are accordingly defined in terms of these flux vectors [7]. Chapman and Enskog independently derived general formulae for transport coefficients, effectively closing the transport equations [6, 8]. The Chapman-Enskog kinetic theory of gases applies strictly only to monatomic gases or species with no internal degrees of freedom, where the interaction potential remains spherically symmetric. However, viscosity and diffusion are unaffected by the presence of internal degrees of freedom, allowing the theory to be applicable for most polyatomic species [7]. Since then, Chapman-Enskog formulations have been generalised and extended to encompass broader molecular models, including those with internal degrees of freedom, ionized gases, and thermo-chemical non-equilibrium.

When deriving transport coefficients for flow simulations, two primary considerations must be addressed. The first is the evaluation of the Chapman-Enskog formulation for multi-species mixtures, which involves lengthy calculations and inverse matrix operations. The second is the determination of collision cross-section terms for all possible species pairs. While the complex calculations required for the first are often simplified through approximations that maintain good accuracy [7, 9], the latter is addressed either by expressing intermolecular potential functions analytically—using models such as the rigid sphere and Lennard-Jones potentials—or by utilising experimental data to infer intermolecular interactions [10, 11]. Additionally, in high enthalpy flows involving molecules, the presence of internal degrees of freedom must be considered. Although viscosity is unaffected by internal modes, thermal conductivity is dependent on the nature of these internal modes [7].

Recent studies on high-temperature transport properties include comparisons of transport property models for Mars entry [12], evaluations of transport properties for ablative heat shields [13], and analyses of diffusion theory for high-temperature multi-species gases [14]. Each of these studies references the Yos mixing rule [9, 15] in conjunction with the collision integral method to derive accurate transport properties, supplemented by integral data from sources such as Gupta et al. [5, 16] or more recent data from Wright et al. [17, 18]. For air-specific species, Palmer and Wright [19] compare four different methods for calculating 11-species air viscosity at high temperatures, assessing both accuracy and computational efficiency. Additionally, four distinct methods are evaluated for computing frozen thermal conductivity [20]. Both studies compare the Yos method with first-order approximations of multi-component mixture viscosity and thermal conductivity, concluding that the Yos model provides excellent agreement for non-ionized or weakly ionized flows.

High-fidelity simulations of boundary layer flows and the transition to turbulence under high enthalpy conditions have included significant contributions by Passiatore et al. [21, 22, 23], who model viscosity and thermal conductivity following Blottner's approach [24]. As will be discussed, Wilke's mixing rule [25], used within this model, requires embedded loops over all species. This process can become computationally expensive in large-scale simulations involving grid resolutions on the order of $10^8 - 10^9$ points. Similarly, studies on high enthalpy channel flows [26], DNS

of transitional boundary layers under high enthalpy [27], and shock standoff distances in hypersonic flows around blunt bodies [28] apply Wilke's mixing rule with various models for species-specific viscosity and thermal conductivity. Other research studies on compressible isotropic turbulence with vibrational non-equilibrium [29, 30] and chemically reacting hypersonic flow simulations [31] have modelled viscosity using Sutherland's law [32] with updated constants.

In this paper, we present and validate a computationally efficient formulation for viscosity and thermal conductivity that offers improvements for DNS/LES applications by balancing accuracy with cost-effectiveness, making it a potentially advantageous alternative to conventional mixing rules. The model is based on a five-species air mixture (O, O_2, N, N_2, NO) and is applicable across temperatures from $100K$ to $9000K$, where ionization effects can be reasonably neglected. The model is subsequently evaluated in simulations of a thermal and chemical non-equilibrium free shear layer flow under high enthalpy conditions.

II. Formulation

The governing equations for fluid flow with thermo-chemical non-equilibrium consist of the continuity, momentum, vibrational and total energy conservation equations [2]. The continuity equations incorporate chemical reaction of the mixture and thermal energy exchange between the ro-translational and vibrational modes. The equations have been simplified to a two temperature representation of the energy modes, where the electronic mode is disregarded and only the five neutral species of air are taken into account.

$$\frac{\partial}{\partial t}\rho_s + \frac{\partial}{\partial x_j}\rho_s u_j = \frac{\partial}{\partial x_j}\left(\rho D_s \frac{\partial X_s}{\partial x_j}\right) + \dot{\omega}_s \tag{1}$$

$$\frac{\partial}{\partial t}\rho u_i + \frac{\partial}{\partial x_j}\rho u_i u_j = -\frac{\partial p}{\partial x_i} + \frac{\partial}{\partial x_j}\left[\mu\left(\frac{\partial u_i}{\partial x_j} + \frac{\partial u_j}{\partial x_i}\right) - \frac{2}{3}\mu\frac{\partial u_k}{\partial x_k}\delta_{ij}\right] \tag{2}$$

$$\frac{\partial}{\partial t}\rho e_v + \frac{\partial}{\partial x_j}\rho e_v u_j = \frac{\partial}{\partial x_j}\left(K_v \frac{\partial T_v}{\partial x_j}\right) + \frac{\partial}{\partial x_j}\left(\rho \sum_{s=1}^{5} e_{v,s} D_s \frac{\partial X_s}{\partial x_j}\right) + \sum_{s=mol} \rho_s \frac{(e^*_{v,s} - e_{v,s})}{\tau_s} + \sum_{s=mol} \dot{\omega}_s e_{v,s} \tag{3}$$

$$\frac{\partial}{\partial t}\rho E + \frac{\partial}{\partial x_j}\rho H u_j = \frac{\partial}{\partial x_j}\left(K_{tr}\frac{\partial T}{\partial x_j} + K_v \frac{\partial T_v}{\partial x_j}\right) + \frac{\partial}{\partial x_j}\left(\rho \sum_{s=1}^{5} h_s D_s \frac{\partial X_s}{\partial x_j}\right) + \frac{\partial}{\partial x_j}\left[u_i \mu\left(\frac{\partial u_i}{\partial x_j} + \frac{\partial u_j}{\partial x_i}\right) - \frac{2}{3}u_i\mu\frac{\partial u_k}{\partial x_k}\delta_{ij}\right] \tag{4}$$

The governing equations rely on three main assumptions [1]. Firstly, the flow is assumed to be as continuum. Secondly, the vibrational energy is assumed to be populated by a Boltzmann distribution, corresponding to a single vibrational temperature for which the Harmonic Oscillator (HO) model is applied. Strictly this is valid for only lower vibrational levels, however the HO model is considered to be sufficient for the present purposes. Thirdly, the energy

modes are represented by two temperatures. The rotational and translational modes are considered to be coupled and hence represented by the translational temperature T. The vibrational mode is represented by the vibrational temperature T_v and there is no temperature representing the electronic mode T_e since ionisation is disregarded.

The pressure is calculated using Dalton's law of partial pressure as

$$p = \sum \rho_s \frac{\mathscr{R}}{M_s} T \quad , \tag{5}$$

where ρ_s is the species density, $\mathscr{R}$ is the universal gas constant, M_s is the species molecular mass and T is the ro-translational temperature. Implementing the Rigid Rotor (RR) and Harmonic Oscillator (HO) model, the enthalpy of the mixture per unit mass is given by

$$\rho h = \sum_s \rho_s \; h_s = \sum_s \rho_s \left(\frac{3}{2} \frac{\mathscr{R} T}{M_s} + \frac{\mathscr{R} T}{M_s} + \frac{\theta_s / T_v}{e^{\theta_s / T_v} - 1} \frac{\mathscr{R} T}{M_s} + \frac{\mathscr{R} T}{M_s} + h^\circ_{f_s} \right) \quad , \tag{6}$$

where $h^\circ_{f_s}$ is the species enthalpy of formation and θ_s is the molecular species characteristic vibrational temperature. Values for M_s, θ_s, and $h^\circ_{f_s}$ were taken from Gnoffo et al. [2]. A five species air composition comprises the five reactions

$$\begin{aligned} N_2 + M &\longleftrightarrow 2N + M \; , \\ O_2 + M &\longleftrightarrow 2O + M \; , \\ NO + M &\longleftrightarrow N + O + M \; , \\ N_2 + O &\longleftrightarrow NO + N \; , \\ NO + O &\longleftrightarrow O_2 + N \; , \end{aligned} \tag{7}$$

where M is the third body representing the other heavy particles. For the finite-rate chemistry, Park's two temperature model (with $\sqrt{TT_v}$ as the forward reacting temperature) is used, with chemical reaction rates given by Park [4] for the dissociation of nitric oxide (NO) into atomic nitrogen (N) and atomic oxygen (O) and Park et al. [33] for all the other reactions. A Landau-Teller formulation of energy exchange is used, with vibrational relaxation rates expressed by Millikan and White [34] with coefficients from Park [4]. For the simulations conducted here, thermal diffusion is disregarded and mass diffusion is modelled using a constant Schmidt number of 0.71 such that $D_s = \mu / (\rho \mathrm{Sc})$, similar to other studies [35, 36]. Comparisons to a full binary diffusion treatment showed negligible differences in the results for the mixing layer cases presented later.

The governing equation require models for fluid properties. Here we focus on the viscosity μ and thermal conductivity K. In the following subsections (II.A to II.E) existing methodologies are explained. Two of these are then used as a reference for developing a single model in subsection II.F that is optimised for temperatures from $100K$ to $9000K$. This

section also provides some important notes on the implementation.

A. Hirschfelder-Lennard-Jones (HLJ)

According to the model of Hirschfelder et al [7], applicable to a lower temperature regime, the viscosity for a single species s and a mixture can respectively be expressed as

$$\mu_s = 266.93 \left(\frac{\sqrt{M_s T}}{\sigma_s^2 \Omega^{(2,2)}(T_s^*)} \right) \times 10^{-8} \tag{8}$$

$$\mu = 10^{-8} \sum_{i=1} \frac{X_i^2}{X_i^2/\mu_i + 2.308 \sum_{k \neq i} \frac{X_i X_k}{A_{ik}^\star \mu_{ik}} \frac{M_k}{(M_i + M_k)}}, \tag{9}$$

with

$$\mu_{ik} = 266.93 \left(\frac{\sqrt{2 M_i M_k T/(M_i + M_k)}}{\sigma_{ik}^2 \Omega_{ik}^{(2,2)}(T_{ik}^*)} \right) \times 10^{-8},$$

where μ_s and μ represent the viscosity of a pure gas and a gas mixture in $(kg/m \cdot s)$ [7]. The force constants ϵ and σ are determined from viscosity measurements along with the quantity $A^\star$. X_s is the mole fraction for species s, M_s is the species molecular weight in grams, and $\Omega_{ik}^{(2,2)}(T_{ik}^*)$ is the collision integral evaluated using the binary reduced temperature T_{ik}^*. The expression given for this model has been simplified by incorporating the assumption that the off-diagonal elements of the full form of viscosity given for the multi-component gas mixtures have little contribution and hence can be overlooked, resulting in a simple form of the rigorous multi-component mixtures viscosity [7]. It was verified that Eq. (9) was in good agreement with the full Chapman-Enskog formulation given by Hirschfelder et al. [7]. The Lennard-Jones model provides a realistic potential function to calculate the transport properties for non-polar molecules when compared to other simple definitions. The collision cross sections, $\Omega^{(i,j)}$, from this model have been devised in the form of tables in terms of the reduced temperature $T^* = kT/\epsilon$ [7]. Additionally, for the binary mixture $\sigma_{ij} = (\sigma_i + \sigma_j)/2$ and $\epsilon_{ij} = \sqrt{\epsilon_i \epsilon_j}$.

The formulation for the coefficient of thermal conductivity is described similarly to that of viscosity

$$K_s = 8.3224 \times 10^{-2} \frac{\sqrt{T/M_s}}{\sigma_s^2 \Omega^{(2,2)}(T_s^*)},$$

$$K_s = \frac{15}{4} \frac{\mathscr{R}}{M_s} \mu_s, \tag{10}$$

where K_s is the coefficient of thermal conductivity for a pure gas in $(W/m \cdot K)$ composed of a monatomic species s, $\mathscr{R}$ is the universal gas constant (here in $cal/K \cdot mole$), and 8.3224×10^{-2} includes the conversion factor from $(cal/cm \cdot s \cdot K)$ to $(W/m \cdot K)$.

To calculate the thermal conductivity of a mixture with polyatomic species, a semi-empirical method is used, since

the thermal conductivity of mixtures is not proportional to the mixture viscosity as seen with a pure gas formulation. This is done by using the formulation for a mixture of monatomic species with correction from experimental data of each molecule. The full formulation for the monatomic mixture, $[K_{mix}]_{mon}$, is given by Hirschfelder et al. [7]. The ratio of the experimental and theoretical (Eq. (10)) result is computed and used in the relation

$$K_{mix} = [K_{mix}]_{mon}[X_1 R_1 + X_2 R_2], \tag{11}$$

with

$$R_i = \frac{(K_i)_{exp}}{(K_i)_{mon}}. \tag{12}$$

To calculate the viscosity and thermal conductivity, the force constants σ and ϵ/k must be defined. The two adjustable parameters are found using experimental data of the substance at two different temperatures. Various studies have provided different parameters for each air species and for air as a whole [7, 8, 37–39]. When using the force constants to compute the viscosity within the lower temperature range, those given by Poling et al. [38] and Hirschfelder et al. [7] align well with Yos-Gupta at around $2000K$ where Yos-Gupta is assumed to be correct. On the other hand, those given by Childs and Hanley [40] and Lemmon and Jacobsen [39] match well with each other but compute slightly higher values of viscosity. For this study, those given by Hirschfelder are used, where two different force constants are provided with temperature limits tailored to be more accurate at their respective temperatures, one below temperatures of $300K$ and other up to $1000K$.

B. Yos-Gupta

When considering air at high temperatures, in most approximations to the Chapman-Enskog formulation the transfer of momentum from one species to other is either neglected or has been replaced by a constant empirical value. However, the model presented by Yos [9] accounts for this interaction. The mixing rule is defined as

$$\mu \text{ or } K_{tr} = \frac{\sum_s X_s/(A_s + a_{av})}{1 - a_{av}\sum_s/(A_s + a_{av})}, \tag{13}$$

where X_s is the species mole fraction, μ and K_{tr} are defined in terms of $(g/cm \cdot s)$ and $(cal/cm \cdot s \cdot K)$ respectively, and a_{av} is the average value of the non-diagonal matrix elements defined as

$$a_{av} = \frac{\sum_{i,j} X_i X_j \left(\frac{1}{A_i} - \frac{1}{A_j}\right)^2 a_{ij}}{\sum_{i,j} X_i X_j \left(\frac{1}{A_i} - \frac{1}{A_j}\right)^2}, \tag{14}$$

$$A_i = \sum_l X_l B_{il}. \tag{15}$$

The parameters a_{ij} and B_{il} are computed differently for viscosity and thermal conductivity. For viscosity, a_{ij} and B_{il} are defined as

$$a_{ij} = \frac{N_A}{(M_i + M_j)} \left[2\Delta_{ij}^{(1)} - \Delta_{ij}^{(2)}\right], \tag{16}$$

$$B_{il} = \frac{N_A}{M_i} \Delta_{il}^{(2)}, \tag{17}$$

where N_A is the Avogardo number in $(mole/g \cdot mole)$ and M_i is the species molecular weight in grams. Also,

$$\Delta_{ij}^{(1)} = 8/3 \times (1.5460 \times 10^{-20}) \left[\frac{2M_i M_j}{\pi \mathscr{R} T (M_i + M_j)}\right]^{1/2} \pi \bar{\Omega}_{ij}^{(1,1)}, \tag{18}$$

$$\Delta_{ij}^{(2)} = 16/5 \times (1.5460 \times 10^{-20}) \left[\frac{2M_i M_j}{\pi \mathscr{R} T (M_i + M_j)}\right]^{1/2} \pi \bar{\Omega}_{ij}^{(2,2)}, \tag{19}$$

where $\mathscr{R}$ is the universal gas constant in $(cal/g \cdot mole \cdot K)$. The collisional integrals $\pi \bar{\Omega}_{ij}^{(1,1)}$ and $\pi \bar{\Omega}_{ij}^{(2,2)}$ are expressed as curve fits in the form

$$\pi \bar{\Omega}_{ij}^{(1,1)} = \exp(D_{11})\, T^{\left[A_{11} \ln(T)^2 + B_{11} \ln(T) + C_{11}\right]}, \tag{20}$$

$$\pi \bar{\Omega}_{ij}^{(2,2)} = \exp(D_{22})\, T^{\left[A_{22} \ln(T)^2 + B_{22} \ln(T) + C_{22}\right]}, \tag{21}$$

where T is the translational temperature and coefficients A_{11}, B_{11}, C_{11}, D_{11}, A_{22}, B_{22}, C_{22} and D_{22} are given by [5].

Assuming Eucken's approximation, the mixture thermal conductivity K can be expressed as

$$K = K_t + K_r + K_v, \tag{22}$$

where K_t is the translational contribution, K_r is the rotational contribution, and K_v is the vibrational contribution to the

thermal conductivity. For the translational thermal conductivity, a_{ij} and B_{il} are defined as

$$a_{ij} = (4.184 \times 10^7) \frac{2M_i M_j}{15k(M_i + M_j)^2} \left[\left(\frac{33}{2} - \frac{18}{5} B^*_{ij} \right) \Delta^{(1)}_{ij} - 4\Delta^{(2)}_{ij} \right], \tag{23}$$

$$B_{il} = \frac{2\ (4.184 \times 10^7)}{15k\ (M_i + M_l)^2} \times \left[8M_i M_l\ \Delta^{(2)}_{il} + (M_i - M_l) \left(9M_i - 15M_l/2 + 18\ B^*_{il}\ M_l/5 \right) \Delta^{(1)}_{il} \right], \tag{24}$$

where k is the Boltzmann constant (in erg/K). Similar to the collision integrals, the ratio B^*_{ij} is given as a curve fit with the form

$$B^*_{ij} = \exp(C)\ T^{[Aln(T)+B]}, \tag{25}$$

with coefficients A, B and C defined by Gupta et al. [5]. The contribution from the internal excitation energy of the molecules can be expressed as

$$K_r = 2.3901 \times 10^{-8} k \sum_i \left[\frac{\left(\frac{(c_{p_i})_{rot}}{\mathscr{R}} \right) X_i}{\sum_j X_j \Delta^{(1)}_{ij}} \right], \tag{26}$$

$$K_v = 2.3901 \times 10^{-8} k \sum_i \left[\frac{\left(\frac{(c_{p_i})_{vib}}{\mathscr{R}} \right) X_i}{\sum_j X_j \Delta^{(1)}_{ij}} \right], \tag{27}$$

$$\tag{28}$$

where $(c_{p_i})_{rot}$ is the rotational contribution to the specific heat of species i and $(c_{p_i})_{vib}$ is the vibrational contribution evaluated by the vibrational temperature (T_v), both expressed in $(cal/g \cdot mole \cdot K)$. For the transport properties defined in this section, conversion factors to SI units are required where $(cal/cm \cdot s \cdot K)$ for thermal conductivity is converted to $(W/m \cdot K)$ by a factor of 418.4 and $(g/cm \cdot s)$ for viscosity is converted to $(kg/m \cdot s)$ by a factor of 0.1.

C. Lemmon and Jacobsen

The formulations for μ and K developed by Lemmon and Jacobsen [39] are derived from a combination of theoretical models for the dilute gas and empirical equations representing the residual contributions from molecular interactions. The equations governing the dilute gas utilise the Chapman-Enskog theory, with polynomial fits for collision integrals that are calibrated to fit experimental data. The improved model proposed by Olchowy and Sengers [41] is employed, while the residual contribution follows an approach similar to that of Lemmon et al. [42]. This results in a formulation that is applicable across all liquid and vapour states. The model uncertainty is given as 2% for nitrogen and 5% for oxygen and air, with somewhat larger deviations near the critical point. In their report, Lemmon and Jacobsen [39]

compare the model predictions with more than 150 sets of experimental data, demonstrating its robustness and accuracy within these uncertainty ranges.

Following this model, the viscosity is expressed using the equation

$$\mu = (\mu_0 + \mu_{re}) \times 10^{-6}, \tag{29}$$

where μ is given in $(kg/m \cdot s)$, μ_0 is the dilute gas viscosity, and μ_{re} is the residual fluid viscosity. The equation for the dilute gas is given as

$$\mu_0 = \frac{0.0266958\sqrt{MT}}{\sigma^2 \Omega^\star}, \tag{30}$$

$$\Omega^\star = \exp\left(\sum_{i=0}^{4} b_i [\ln(T/(\epsilon/k))]^i\right), \tag{31}$$

where M is the molecular mass in grams, T is the translational temperature, σ is the force constant and $\Omega^\star$ is the collision cross section fitted to experimental data with constants given by Lemmon and Jacobsen [39].

The thermal conductivity is expressed using the equation

$$K = K_0 + K_{re} + K_c, \tag{32}$$

where K_0 is the dilute gas thermal conductivity, K_{re} is the residual fluid thermal conductivity, and K_c is the thermal conductivity critical enhancement. The dilute gas thermal conductivity is given as

$$K_0 = N_1 \left[\mu_0 \times 10^{-6}\right] + N_2 \left(\frac{T_c}{T}\right)^{t_2} + N_3 \left(\frac{T_c}{T}\right)^{t_3}, \tag{33}$$

where T_c is the critical temperature, μ_0 is the dilute gas viscosity given in $N.s/m^2$ and N_1, N_2, N_3, t_2, t_3 are species specific constants given in [39].

If a dilute gas is considered, where particle interactions are negligible (typically at low pressures and high temperatures), the critical and residual enhancements (see [39] for details) can be neglected due to sufficiently low density. In this study, the contributions of residual and critical enhancements were found to be minimal and have therefore been neglected.

D. Blottner

Blottner et al. [24] compute the viscosity and thermal conductivity of a gas mixture using Wilke's semi-empirical mixing rule [25], where the viscosity of each individual species is evaluated through polynomials. These curve fits are based on data from Yos [9], Yun and Mason [10], effectively representing Yos's curve fits. The curve-fitting relation for

viscosity is given in the form

$$\mu_s = 0.1 \exp(C)\ T^{[A \ln(T)+B]}, \tag{34}$$

where A,B and C are coefficients given in [24], T is the translational temperature and the constant 0.1 is the converting factor to SI units of $(kg/m \cdot s)$. The species thermal conductivity is expressed in terms of viscosity with Euken's molecular correction factor given in the form

$$K_s = \frac{\mu_s}{M_s}\left[c_{p_s}\frac{M_s}{\mathscr{R}} + 1.25\right], \tag{35}$$

where M_s is the species molecular weight in grams, c_{p_s} is the species specific heat and $\mathscr{R}$ is the universal gas constant. The mixing rule is then expressed in terms of

$$\mu = \sum_{i=1}^{s} \frac{X_i \mu_i}{\sum_{j=1}^{s} X_j \phi_{ij}}, \tag{36}$$

$$K = \sum_{i=1}^{s} \frac{X_i K_i}{\sum_{j=1}^{s} X_j \phi_{ij}}, \tag{37}$$

where X_i is the species mole fraction and

$$\phi_{ij} = \left[1 + \sqrt{\frac{\mu_i}{\mu_j}}\left(\frac{M_j}{M_i}\right)^{1/4}\right]^2 \left[\sqrt{8}\sqrt{1 + \frac{M_i}{M_j}}\right]^{-1}. \tag{38}$$

The mixture rule used in this method has been noted to give inappropriate results for partially ionised gases and deviate from other valid results for temperatures above $10,000K$. Therefore, Blottner's method is only recommended to be used for non- or slightly-ionised gases [24].

E. Sutherland

The Sutherland model represents the molecules as rigid spheres with the addition of a weak attractive force when the spheres are not in contact. While this model is rather crude from a theoretical perspective, it does provide a more rapid variation of viscosity than the simpler rigid sphere model [43]. The viscosity of a gas to a first approximation using this model is given by

$$\mu = \mu_{exp}\left(\frac{T}{T_{exp}}\right)^{3/2}\frac{T_{exp} + S}{T + S}, \tag{39}$$

where μ_{exp} represents the experimental viscosity at temperature T_{exp}, and S is the Sutherland constant, which quantifies the strength of the attractive intermolecular forces, being proportional to the mutual potential energy between

two molecules in contact [8]. The constants used in this work are those given by Hirschel [44], where S is 110.4, $\mu_{exp} = 1.846 \times 10^{-5}\ kg/(m \cdot s)$ and $T_{exp} = 300K$.

F. Present Model

In high-enthalpy flows aimed at simulating hypersonic conditions, extensive calculations are required to produce accurate transport properties, such as those in the model provided by Yos [9], which can significantly increase the overall computational time and resources. Additionally, these models do not accurately represent transport properties at lower temperatures. As a compromise between performance and accuracy, more precise viscosity and thermal conductivity models across their respective temperature ranges have been approximated using simpler polynomial expressions, with coefficients valid for temperatures ranging from $100K$ to $9000K$.

The polynomial for the present model is expressed in the form

$$\Phi = \frac{\sum\limits_{i=atom} 15X_i + \sum\limits_{i=mol} 30X_i}{P(a,b,c,d) \sum\limits_{i=atom} X_i + P(e,f,g,h) \sum\limits_{i=mol} X_i}, \tag{40}$$

with

$$P(A,B,C,D) = |A + B\ T^2 + C\ \ln(T) + D/T|, \tag{41}$$

where X_i is the species mole fraction and coefficients a, b, c, d, e, f, g are given in Table 1. The split into summed atom and summed molecular contributions and the omission of a separate mixing rule simplifies the final form.

As mentioned earlier, for a more complete definition of thermal conductivity, the total thermal conductivity can be decomposed into different modes as

$$K = K_t + K_r + K_v,$$

where K_t represents the contribution from the translational mode of the species, K_r from the rotational mode, and K_v from the vibrational mode. In modelling high-enthalpy effects, particularly for non-equilibrium air at temperatures below $9000K$, among these three contributions to frozen thermal conductivity, the rotational mode can reasonably be assumed to couple with the translational mode and is therefore governed by the translational temperature, while the vibrational contribution is governed by the vibrational temperature. Consequently, given the correspondence of the provided expressions to air at temperatures below $9000K$, in the present model the thermal conductivity is expressed in terms of K, K_{tr}, and K_v, which represent the total thermal conductivity, the ro-translational thermal conductivity, and the vibrational thermal conductivity, respectively. The total thermal conductivity and ro-translational thermal

Table 1 Coefficients for viscosity and thermal conductivity for the present model.

	a	b	c	d	e	f	g	h
μ	-2.0989e+05	-5.2310e-06	1.9855e+04	-2.7244e+08	1.2667e+06	3.3933e-04	-1.3007e+05	3.5234e+08
K	3.2315e+02	2.1022e-07	-3.5288e+01	8.0676e+04	-4.5599e+02	-1.8431e-07	4.6392e+01	-3.0308e+05
K_{tr}	2.1762e+02	2.1403e-07	-2.4067e+01	1.0838e+05	-9.8842e+02	-5.1961e-07	1.0492e+02	-2.3396e+05

Table 2 Coefficients for the species vibrational thermal conductivity.

	A	B	C	D	E	F	G
K_{v,N_2}	1.9200e-04	-3.9290e-06	1.4026e-08	-4.8403e-12	7.5275e-16	-5.0128e-20	1.0884e-24
K_{v,O_2}	-1.1446e-03	7.2095e-06	6.2555e-09	-2.6587e-12	4.2901e-16	-2.5152e-20	3.0436e-25
$K_{v,NO}$	-4.2658e-04	9.8630e-07	1.1229e-08	-4.2799e-12	7.0384e-16	-4.8694e-20	1.1027e-24

conductivity are both defined using the expression provided in Eq. (40), while the vibrational thermal conductivity for each species is defined using sixth-order polynomials in the form

$$K_{v_i} = |X_i \ \left[A_i + B_i\, T_d + C_i\, T_d^2 + D_i\, T_d^3 + E_i\, T_d^4 + F_i\, T_d^5 + G_i\, T_d^6\right]|, \tag{42}$$

where T_d is defined as $\sqrt{TT_v}$ and the coefficients $A_i, B_i, C_i, D_i, E_i, F_i, G_i$ are given in Table 2 separately for each molecular species. To calculate the total vibrational thermal conductivity (K_v) the species vibrational mode can be summed as

$$K_v = \sum_{i=mol} K_{v_i}. \tag{43}$$

Following Eucken's expression for total thermal conductivity, one can also calculate the ro-translational thermal conductivity by subtracting the vibrational contribution

$$K_{tr} = K - \left(\sum_{i=mol} K_{v_i}\right). \tag{44}$$

The polynomial given as Eq. (40) separates the contributions to transport properties between molecules and atoms. This division enables a more accurate representation of transport properties in chemically non-equilibrium flows, where the composition deviates from the equilibrium composition for which they were optimised. Additionally, the polynomial given as Eq. (42) is in standard form without division between species, as atoms do not contribute to vibrational modes.

The selected polynomial forms and their coefficients were optimised to accurately represent the respective transport properties across equilibrium and various non-equilibrium flow states for temperatures ranging from $100K$ to $9000K$. The

reference data used for the optimisation included equilibrium compositions between temperatures $100K$ to $9000K$ and four additional frozen compositions for temperatures $1000K$ to $9000K$, representing highly chemically non-equilibrium states. Data points across this temperature range were weighted toward lower temperatures to improve alignment in this region. The selection of equilibrium composition only for temperatures below $1000K$ allows for greater accuracy in this range, as non-equilibrium states are less likely to occur at these temperatures in practical cases. Meanwhile, selecting frozen chemistry data for temperatures above $1000K$ improves the fit for chemically non-equilibrium states. As a result, Eq. (40) is used to define the total viscosity, total thermal conductivity, and ro-translational thermal conductivity, while Eq. (42) is used to define the species vibrational thermal conductivity, with the capability to represent total vibrational thermal conductivity through Eq. (43).

When establishing a reference value for the data, the Hirschfelder-Lennard-Jones (HLJ) model was chosen for viscosity between $100K$ and $1400K$, while the Yos-Gupta model was used from $1400K$ to $9000K$. Hirschfelder et al. [7] demonstrate that the Lennard-Jones potential is one of the more accurate models for gases up to $1100K$, given the appropriate force constants are applied. The collision integrals in the Yos-Gupta method correlate directly with data from Yun et al. [11] and Vanderslice et al. [45], reported to be accurate from $1000K$ to $15,000K$. This combination is therefore assumed to provide a good reference over the entire temperature range.

For thermal conductivity, the HLJ model was used from $100K$ to $700K$ applying the semi-empirical method of Hirschfelder et al. [7], with correction factors for each species provided by the model from Lemmon and Jacobsen [39]. Given that air composition in this range is a combination of N_2 and O_2 only, the gas was assumed to be a binary mixture. The semi-empirical method, combined with correction factors, was selected due to limited theoretical models for mixture thermal conductivity with polyatomic species; thus, thermal conductivity is calculated as a mixture of monatomic species, with vibrational contributions added through experimental data. Notably, Eucken's correction factor for polyatomic species does not yield acceptable results for mixture thermal conductivity [7]. The Lemmon-Jacobsen model [39] used for experimental data representation was reduced by 0.5% for N_2 to better fit temperatures above $300K$. The default Lemmon-Jacobsen model and its accuracy compared to experimental data are provided by Lemmon and Jacobsen [39]. For temperatures between $700K$ and $9000K$, the Yos-Gupta model was used.

Thus, while the overall model selection was guided by accuracy within each range, the exact temperature boundaries were set where the models intersect, resulting in a smoother overall representation of the transport properties and better alignment when optimising polynomial coefficients. A standard least squares method was used for the optimisation.

Comments on implementation

Table 3 presents a selection of calculated properties at various temperatures, along with their corresponding compositions. The compositions were chosen to be close to the equilibrium composition at each respective temperature. To calculate the mixture viscosity, Eq. (40) should be used with the respective coefficients provided in Table 1. This

Table 3 Results from the present model for code verification.

T	X_O	X_{O_2}	X_N	X_{N_2}	X_{NO}	μ	K	K_{tr}	K_v
100	0.00	0.21	0.00	0.79	0.00	7.1580e-06	9.1655e-03	1.0545e-02	1.2805e-04
298	0.00	0.21	0.00	0.79	0.00	1.7564e-05	2.4819e-02	2.5514e-02	4.2750e-04
2000	0.01	0.20	0.00	0.78	0.01	6.5898e-05	1.1750e-01	9.6982e-02	2.0617e-02
5000	0.33	0.00	0.03	0.62	0.02	1.3187e-04	2.5485e-01	2.1730e-01	3.6434e-02
9000	0.21	0.00	0.78	0.01	0.00	2.4960e-04	5.3366e-01	5.2967e-01	1.2956e-03

formulation covers both equilibrium and non-equilibrium states. For thermal conductivity, it can be noted that the fitting process results in values of K that are not exactly equal to the sum of K_{tr} and K_v, particularly at the extremes of the temperature range. The most accurate results can be achieved by taking into account whether the flow is in equilibrium, in weakly non-equilibrium, or in a strongly non-equilibrium state. The recommended approaches are as follows:

1) Equilibrium State: For thermally equilibrium simulations, where heat flux is expressed in terms of the derivative of a single temperature in the governing equations, a single expression for total thermal conductivity, as defined by Eq. (40) with K coefficients from Table 1, is sufficient.
2) Weakly Non-Equilibrium State: For thermal non-equilibrium simulations in which the translational, rotational, and vibrational contributions to thermal conductivity are expressed separately using derivatives of translational and vibrational temperatures, K should be expressed in terms of K_{tr} and K_v. Under near thermal and chemical equilibrium conditions, it is recommended to use Eq. (43) for K_v, and Eq. (44) for K_{tr}.
3) Strongly Non-Equilibrium State: For highly chemical and thermal non-equilibrium states, Eq. (40) should be used for K_{tr}, and Eq. (43) for K_v, with an added correction factor for K_{tr} defined as:

$$K_{tr} = \Phi - |\ 2.03\ (T - T_v)\ T \times 10^{-10}| \tag{45}$$

where Φ is the prediction from Eq. (40). This correction insures a better agreement of the ro-translational thermal conductivity in thermal non-equilibrium states by incorporating the vibrational temperature in the formulation.

The practical cases that follow will give a better representation of what conditions can be classified as being close to equilibrium. If the extent of non-equilibrium condition cannot be estimated in advance, then the third option can be used, which gives a maximum error of 14% at $100K$ and below 4% for temperatures above $200K$ in cases where the flow is in equilibrium.

III. Results

The proposed model from the previous section is evaluated for accuracy against the existing models for a series of tests. Firstly, the ability to reproduce property values in thermal and chemical equilibrium is demonstrated. Secondly, a 0D heat bath case is used to study strong non-equilibrium states with no fluid motion. Thirdly, numerical simulations of 2D and 3D mixing layer case in non-equilibrium are considered. Finally, the computational savings are demonstrated.

A. Model evaluation in equilibrium

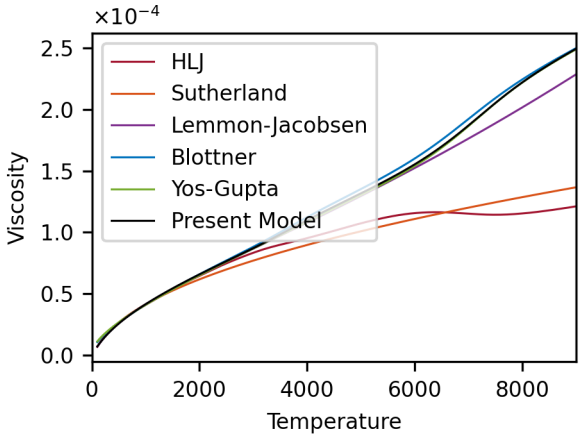

(a) Viscosity against temperature for the full temperature range.

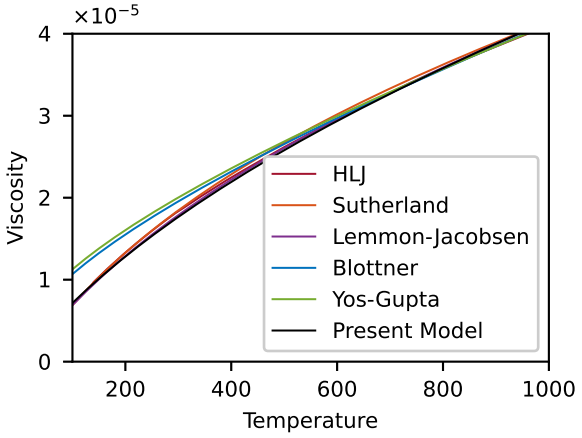

(b) Viscosity against temperature for lower temperatures.

Fig. 1 Comparison of viscosity of the present model against other models for thermo-chemical equilibrium air.

Figure 1a shows the viscosity of a five-species air mixture at atmospheric pressure in thermal and chemical equilibrium, calculated using various models across a temperature range of $100K$ to $9000K$. The present model (equilibrium formulation) is shown with the solid black line. A subset of the same data is shown in Fig. 1b, focusing on the lower temperature range, from $100K$ to $1000K$. It is evident that no single existing model can accurately capture

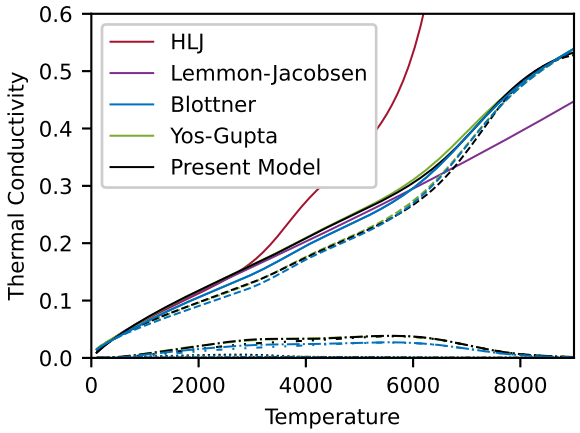

(a) Thermal conductivity against temperature for the full temperature range.

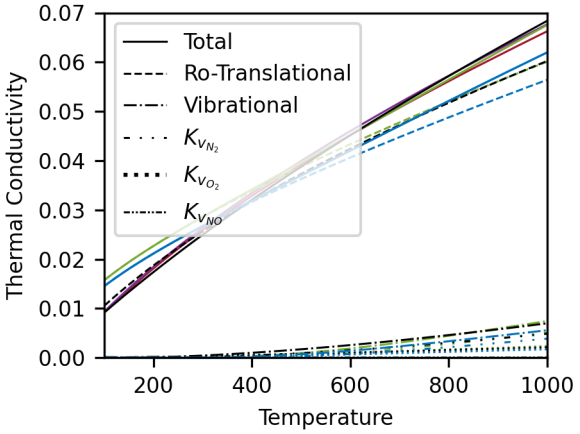

(b) Thermal conductivity against temperature for lower temperatures.

Fig. 2 Comparison of thermal conductivity of the present model against other models for thermo-chemical equilibrium air. The colour scheme is given in the legend in (a) and the linestyle is given in the legend in (b).

viscosity over the entire temperature range, with the HLJ and Sutherland models having large errors at high temperatures and the Yos-Gupta and Blottner models having significant errors at low temperatures. It is also notable that the Blottner and Yos-Gupta models diverge from each other at higher temperatures, specifically between $4000K$ and $8000K$. In contrast, the present model aligns closely with the selected reference models across each temperature segment, showing strong agreement with the HLJ model for temperatures below $1000K$ and the Yos-Gupta model for temperatures above this threshold.

Figure 2a (over the full temperature range) and Fig. 2b (for lower temperatures) shows the present model alongside other thermal conductivity models, highlighting the distinct contributions to thermal conductivity from ro-translational and vibrational modes. Note that the line colour is shown in the legend for part (a) of the figure and the line style in the legend for part (b). Significant discrepancies are observed between the results computed by Blottner, Yos-Gupta, and HLJ.

Similar to the viscosity comparison, there is a clear divergence between the Blottner and Yos-Gupta models at higher temperatures, as well as between HLJ and the other two models at lower temperatures. Additionally, the vibrational contribution to thermal conductivity in the Blottner model shows a larger discrepancy compared to Yos-Gupta and HLJ, as Blottner's model uses the Eucken correction factor, which is less accurate than semi-empirical or experimental data-based methods like Yos-Gupta and HLJ.

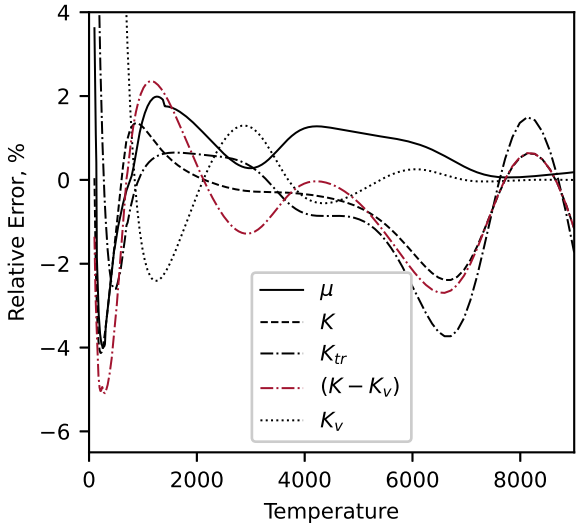

Fig. 3 Error of each property against the respective reference model at each temperature.

Figure 3 presents the relative percentage error of the present model, compared to the reference models across the whole temperature range. In comparison to the reference models, the present model for viscosity exhibits relatively higher errors at lower temperatures, with a maximum error of 4% at $300K$ relative to HLJ, and an error below 2% for temperatures above $400K$ relative to Yos-Gupta. The total thermal conductivity K calculated using Eq. (40) demonstrates small errors, with a maximum error of 4% at around $200K$. The ro-translational thermal conductivity K_{tr} shows a maximum error of 14% at $100K$, but remains below 4% for temperatures above $200K$. Additionally, calculating K_{tr} using Eq. (44) yields a maximum error of 5% at $300K$. Errors in K_v at temperatures below $800K$ can be disregarded, as $K_v \ll K_{tr}$.

Figure 4 presents the Prandtl number, $Pr = c_p\mu/K$, calculated using the transport properties from the present model alongside those in the literature, which are based on empirical or experimental data. For the comparisons, the specific heat for air was calculated using the NASA-9 polynomials [46]. The choice of force constants in the Lennard-Jones model for viscosity calculations significantly influences the alignment with various data sources. For example, the force constants provided by Hirschfelder et al. [7] align well with Hilsenrath et al. [47], while those by Lemmon and Jacobsen [39] are naturally compatible with the Lemmon-Jacobsen model. The Prandtl number for air reported by Cengel et al.

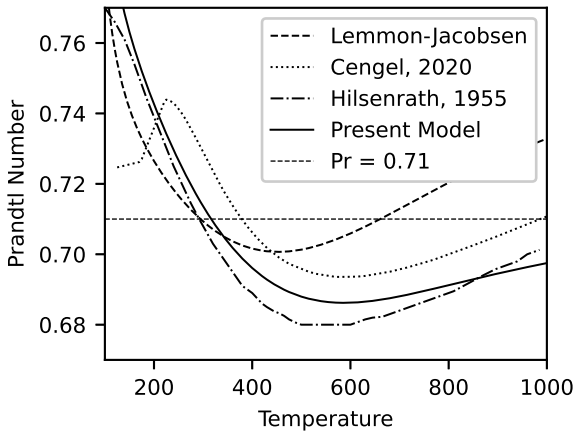

(a) Prandtl number against temperature for lower temperatures.

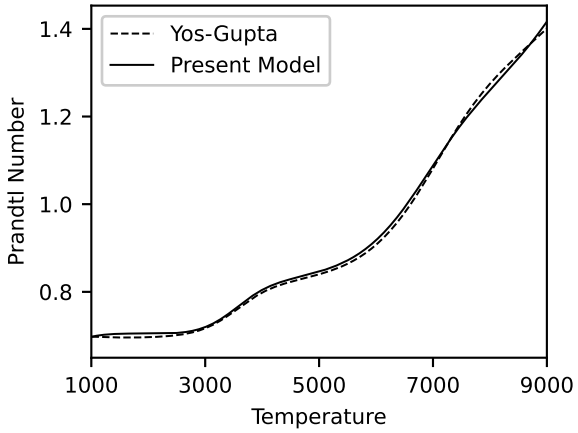

(b) Prandtl number against temperature for higher temperatures.

Fig. 4 Comparison of Prandtl number from the present model against other data.

[48] follows a trend similar to that of the present model, albeit with a slight shift. Given the considerable spread in experimental data above $400K$ and the noticeable differences between the derived transport properties of the Yos-Gupta model and the Lemmon-Jacobsen data, the Prandtl number calculated from the present model is considered to fall within the range of available data.

Additional evaluations were performed to assess the accuracy of the present model under different pressures and to examine its robustness in calculating the transport properties for arbitrary chemical compositions. These are shown in Appendix A.

B. Model evaluation in thermo-chemical non-equilibrium (0D heat bath)

As a first test of non-equilibrium, a 0D heat bath is used. This is a simple configuration with the fluid at rest, which is useful to show how the viscosity and thermal conductivity of the fluid change under the influence of chemical reactions

and vibrational relaxation. To assess the performance of the transport property models (using Eq. (45)), a heat bath simulation was conducted in which the flow initially exists in a state of strong thermal and chemical non-equilibrium state and then relaxes toward equilibrium. The simulation starts with a standard air composition at atmospheric pressure, with the vibrational temperature set as $300K$, the density as $0.05kg/m^3$, the simulation pressure set to $100000Pa$ and the simulation time-step was set to $2.0 \times 10^{-8}s$. The corresponding translational temperature is around $7000K$, putting the flow into severe non-equilibrium. Time advancement was conducted with both 3rd and 4th order Runge-Kutta (RK) schemes, concluding that the 4th order scheme handled the initial highly non-equilibrium chemical relaxation with more precision. The results shown used the 4th order RK scheme with the time step given above.

Figure 5 illustrates various flow parameters as they evolve over time t towards equilibrium using implementation (3) from Sec. II.F. Figure 5a shows the mole fraction of each air species. As the simulation begins in a chemically non-equilibrium state, chemical reactions start to occur and the molecules dissociate, also forming NO. Figure 5b displays the translational and vibrational temperatures, highlighting the transition from an initial vibrational non-equilibrium state to equilibrium. The overshoot of the vibrational temperature above the translational temperature, followed by the final relaxation to equilibrium, is attributed to the ongoing chemical reactions. The markers for Fig. 5a and 5b are the same parameters calculated with half the time-step, showing the same results with errors of the order 0.008% and hence presenting a validation of the time advancement scheme.

The calculated viscosity and thermal conductivity are shown in Fig. 5c and Fig. 5d during the simulation. Different line styles in both figures represent various models, while in Fig. 5d, different colours indicate the different contributions to thermal conductivity. The values of both transport properties using the present model closely follow the same trends as results obtained using the Yos-Gupta and Blottner models. As the flow tends to the final equilibrium state, the results are in very close agreement with Yos-Gupta model. Throughout the non-equilibrium region the results of the present model are closer to Yos-Gupta than the Blottner model, even though the present model consists of a simplified mixing rule.

C. Model evaluation for 2D and 3D mixing layers

Mixing layers are examples of inhomogeneous flows that have been used to study the properties of compressible turbulence [49, 50]. Starting from a laminar flow a transition to turbulence starts from a Kelvin-Helmholtz instability, caused by the inflectional nature of the initial velocity profile [51]. In this study a temporally evolving mixing layer, periodic in the streamwise direction, is constructed in 2D and 3D computational domains. The initial velocity profile is configured as two uniform flows in opposite directions, defined by a hyperbolic profile where a disturbance is then

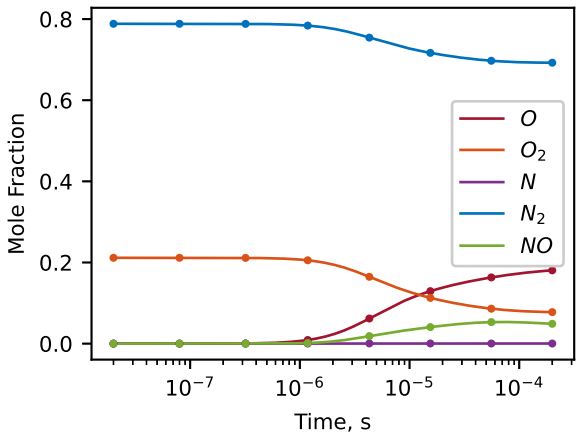

(a) Mole fraction of each species.

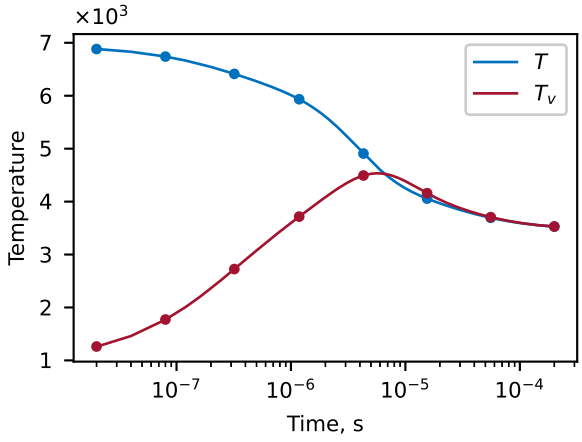

(b) Relaxation of translational and vibrational temperatures.

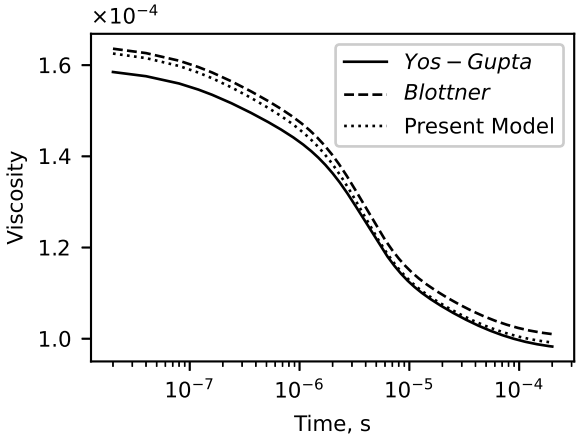

(c) The viscosity calculated at each iteration.

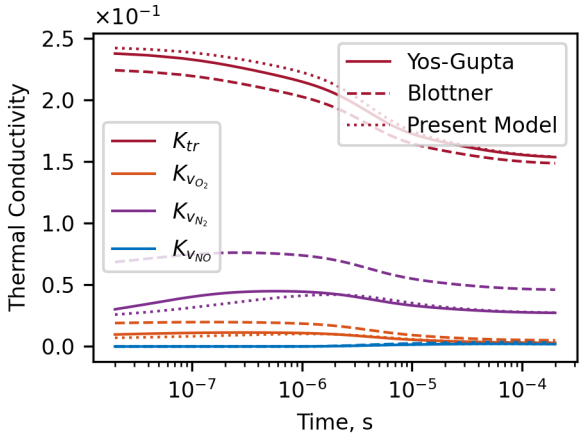

(d) The thermal conductivity calculated at each iteration.

Fig. 5 Heat bath simulation.

superimposed via the v-component of velocity. These components are defined as

$$u = u_\infty \tanh\left(\frac{2y}{\delta_\omega}\right), \tag{46}$$

$$v = 0.01 u_\infty \cos\left(\frac{2\pi x}{L_x}\right) e^{-(y/\delta_\omega)/10}, \tag{47}$$

where u_∞ is the free stream velocity, y is the cross-stream direction, δ_ω is the vorticity thickness, x is the streamwise direction and L_x is the length of the domain in the x direction. Temperature is initially constant everywhere, equal to the free-stream temperature.

The simulations are carried out using OpenSBLI [52], an open-source finite difference flow solver. The spatial and temporal discretisation of the equations is performed using a fourth-order central differencing scheme for space and a fourth-order Runge-Kutta method for time. The code is open source and has been extensively validated, as documented

in Lusher et al. [52, 53] and references therein. In addition, Chapelier et al. [54] compared seven different compressible flow solvers for a compressible Taylor-Green problem, showing excellent agreement across codes that used different numerical methods. For the present simulation, the initial conditions and problem specifications are defined in Table 4. The chemical composition of the flow was set to near equilibrium. The simulation employed periodic boundary conditions in the x direction, while extrapolation boundary conditions were applied at the base and top of the domain. The domain length in the x direction (L_x) was set to $0.044m$, and in the y direction (L_y) to $0.197m$, to minimize the influence of acoustic wave reflections on the mixing process. The grid resolution was configured as 180×325 points in the x and y directions, respectively, with a hyperbolic stretch factor applied in the y direction to concentrate the spatial resolution where needed. The grid was determined after an initial sensitivity study, with grid sensitivity shown later for the more challenging 3D case. Additionally, a binomial filter was employed at the upper and lower boundaries of the domain to attenuate acoustic waves, effectively simulating a quiet free-stream environment. For modelling the mixing layer cases, the third method described in Sec. II.F was utilised.

Table 4 Initial conditions for the shear layer case.

u_∞	ρ_∞	p_∞	Δt	δ°_ω	Y°_O	Y°_{O2}	Y°_N	Y°_{N2}	Y°_{NO}
740 m/s	0.02 kg/m^3	53 kPa	7.0×10^{-8} s	2.961957 mm	0.208	0.003	0.226	0.562	0.001

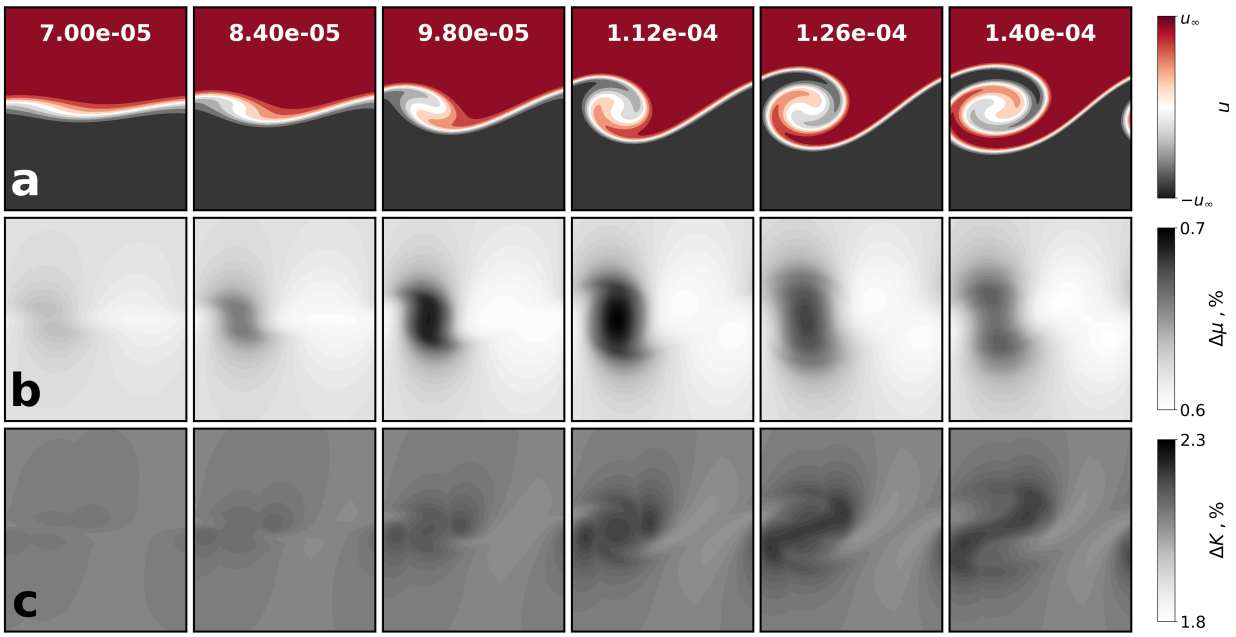

Fig. 6 Error in viscosity and thermal conductivity of present model compared to the Yos-Gupta model, each column depicting a different time (s). a) Passive scalar, b) Error in viscosity, c) Error in total thermal conductivity.

Figure 6 illustrates the development of the 2D mixing layer with each panel representing the same spatial domain.

Each column corresponds to a different time step in the simulation and each row illustrates a different parameter. Row "a" shows the passive scalar, providing a visual representation of the vortex roll-up evolution. As the vortex forms, the core temperature of the vortex decreases while the stagnation point temperature rises. There is minimal chemical reaction (less than 3% change in composition), primarily involving the dissociation of N_2 into N in regions where temperature changes occur. Given the fast chemical reaction timescales relative to flow timescales, the simulation can be considered to be locally in chemical equilibrium. Thermal non-equilibrium is primarily concentrated in the vortex core and in regions of flow expansion and compression, where the vibrational temperature lags behind the translational temperature. Row "b" of Fig. 6 gives the absolute value of the percentage relative difference in viscosity across the flow field, calculated by comparing Yos-Gupta with the present model. Row "c" displays the corresponding percentage difference in total thermal conductivity, comparing Yos-Gupta with the present model. The present model achieves a maximum error of 0.7% for viscosity and 2.2% for thermal conductivity. In terms of error distribution, row "b" primarily reveals that the maximum deviation is located in the vortex core. Regarding thermal conductivity, row "c" displays similar trends to that observed in viscosity, with additional errors in regions of thermal non-equilibrium where the vibrational temperature is elevated compared to the translational temperature. For comparison, the Blottner model showed much larger maximum errors of 4.0% and 7.1% for viscosity and thermal conductivity, respectively.

Figure 7 illustrates a 3D mixing layer under the same conditions as the 2D case study. Here, periodic boundary conditions are applied to the lateral boundaries of the domain, while the top and bottom boundaries are set to extrapolation, similar to the 2D configuration. The initial conditions defining the flow profile and the imposition of the disturbance are given by

$$u = u_\infty \tanh\left(\frac{2y}{\delta_\omega}\right), \tag{48}$$

$$v = 0.05u_\infty \cos\left(\frac{2\pi x}{L_x}\right)\cos\left(\frac{2\pi z}{L_z}\right)\exp\left[-\left(\frac{y}{\delta_\omega}\right)/10\right], \tag{49}$$

$$w = 0, \tag{50}$$

where L_z is the length of the grid in the z direction and w is the initial velocity in the z direction. The temperature is initialized equal to the free-stream temperature. The grid resolution was chosen as $220 \times 385 \times 220$ points for the x,y and z directions respectively. The domain length in the z direction was set identical to the x direction, $0.044m$. Figure 7a displays the Q-criterion as iso-surfaces set at $6 \times 10^{10} s^{-2}$, with thermal non-equilibrium contours on the iso-surfaces. The thermal non-equilibrium contour is defined as the difference between the vibrational and translational temperatures ($T_v - T$), illustrating the degree of thermal non-equilibrium in the flow field. Regions depicted in red correspond to thermally hot states (higher vibrational temperature), while blue regions indicate thermally cold states (higher translational temperature). By the end of the simulation at $t = 2.8 \times 10^{-4}$s shown on Fig. 7a , large-scale vortices have

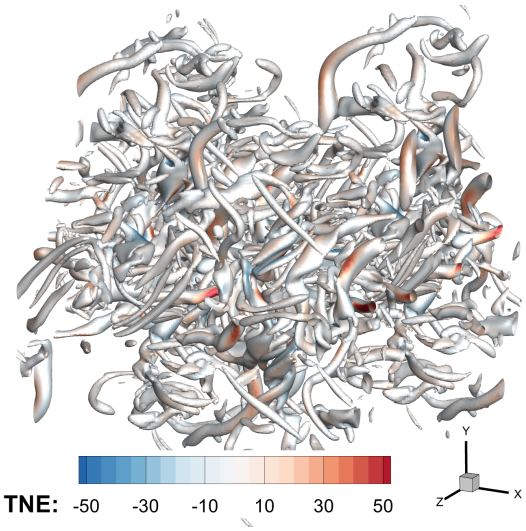

(a) Colour contours of thermal non-equilibrium $(T_v - T)$ superimposed on a Q-Criterion iso-surface at time $2.8 \times 10^{-4} s$.

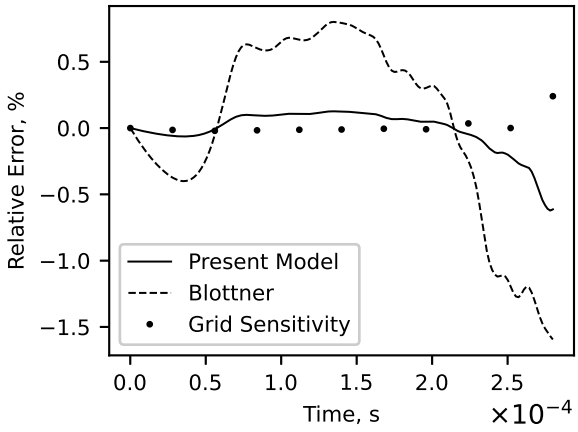

(b) Relative error of momentum thickness in percentage relative to Yos-Gupta, with dots showing the grid sensitivity of the Yos-Gupta results based on a fine grid simulation.

Fig. 7 Three dimensional simulation of the mixing layer and comparison between the transport models.

broken down into small scales. Figure 7b compares the error in non-dimensional momentum thickness of the Blottner model and the present model relative to the Yos-Gupta model, a quantity reflective of the characteristics of developing shear mixing layers. Consistent with the 2D simulation results, the Blottner model shows larger discrepancies compared to the Yos-Gupta method, whereas the present model closely aligns with Yos-Gupta. The markers present in this figure are the respective parameter for a case with a denser grid by a factor of 1.6 in each direction, demonstrating the grid sensitivity and validating the grid convergence for the case studies carried out. As shown, the grid is converged with close to zero percent error during the mixing layer development, with the additional slight deviation in the dissipation region which is reflective of the different turbulence structures being formed based on the grid density. It should be noted that by the end of the simulation the turbulence has lost its determinism, meaning that small changes in initial

condition are amplified sufficiently to break the spanwise symmetry. Thus, the larger errors at later times in Fig. 7 reflect the changing nature of the simulated turbulent flow, from deterministic to stochastic, rather than increased sensitivity to the grid or errors in the property modelling.

This case provides a representative example of a three-dimensional flow with the presence of high-enthalpy effects, enabling the evaluation of the present model for determining transport properties.

D. Computational performance

To assess the computational cost of the models, simulations were conducted on a single computational node using a single NVIDIA A100 GPU. The computational cost was measured by the run time, excluding input/output. Figure 8 presents the computing times for the different viscosity and thermal conductivity formulations used in the 2D and 3D cases. Any difference in performance reflects the combined efficiency gained from both viscosity and thermal conductivity coefficients.

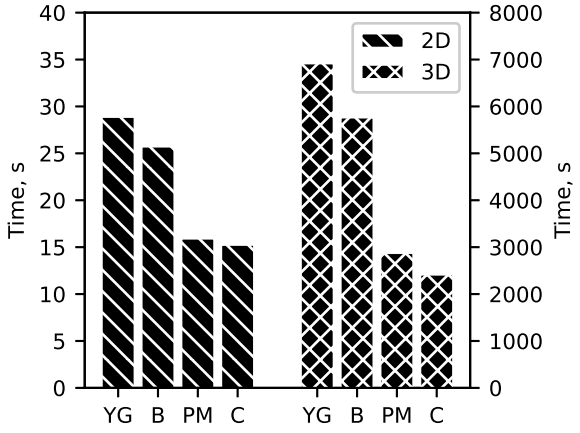

Fig. 8 Computational cost of each model for a 2D and 3D mixing layer simulation, given in terms of time. YG: Yos-Gupta, B: Blottner, PM: Present Model, C: Constant Transport Property.

The present model demonstrated a 45% improvement in efficiency for 2D simulations compared to the Yos-Gupta model, while the Blottner model showed an 11% improvement. For the 3D cases, the present model exhibited 58.5% greater efficiency, while the Blottner model achieved a 16.7% increase relative to the Yos-Gupta model. Additionally, the simulations were conducted with a constant viscosity and thermal conductivity as a reference. These improvements were achieved using a finite difference code optimised in nearly every computational aspect (including work array storage reduction, exploiting the automatic code generation [55]), making the contribution of transport property calculations to overall performance comparatively significant. Given the number of operations required to compute viscosity and thermal conductivity coefficients in the Yos-Gupta model, the contribution to the overall computational time is substantial. Reductions in the relative performance figures would be expected for applications where shock capturing is

required. Nevertheless, the increased performance and consistent levels of accuracy over a wide temperature range make the present model attractive for use in scale-resolving simulations.

IV. Conclusion

The purpose of this paper was to develop a streamlined, efficient model for viscosity and thermal conductivity that balances accuracy with computational performance. This model is intended for five-species air (O, O_2, N, N_2, NO) in thermal and chemical non-equilibrium flow conditions. The model utilises eight coefficients for viscosity and total thermal conductivity, expressed as functions of species mole fraction and temperature. The vibrational contribution to thermal conductivity is represented by a sixth-order polynomial. To align with high-enthalpy non-equilibrium governing equations, the contributions from translational and rotational modes to thermal conductivity are combined into a single term, while the vibrational contribution is specified for each molecular species separately. The separation between molecular and monatomic contributions enhances accuracy for chemical non-equilibrium flows.

In terms of accuracy for equilibrium air at atmospheric pressure, the proposed viscosity model demonstrated only a 4% worst-case error at lower temperatures and below 1.5% error for temperatures above $3000K$ relative to the reference model. The total and ro-translational thermal conductivity exhibited errors below 4% for temperatures above $300K$. Additionally, the Prandtl number computed using the proposed model displayed an error of 1.5% for temperatures between $150K$ and $3000K$ with maximum error of 3.5% when compared to the Prandtl number evaluated using the reference model. To further assess the model's performance in more practical situations, additional test cases were conducted. Firstly, a heat bath case with highly thermal and chemical non-equilibrium states was considered, and secondly, a free shear layer case was simulated in both 2D and 3D, with the latter test case including transition to turbulence. In the 0D heat bath case, the proposed model was more accurate than the Blottner model when compared to the Yos-Gupta model. For the 2D mixing layer case, the proposed viscosity model showed a maximum error of 0.7% through the simulation, compared to Blottner's 4.0%. For thermal conductivity, the proposed model had a maximum error of 2.2%, while Blottner's model showed an error of 7.1%. These case studies confirm that the proposed model effectively represents transport properties in non-equilibrium flows.

In terms of computational performance, the proposed model was 45% more efficient in 2D simulations of a mixing layer compared to the Yos-Gupta model, while the Blottner model achieved only an 11% improvement in efficiency. For 3D simulations, the proposed model was 58.5% more efficient than Yos-Gupta, with Blottner's model, achieving a 16.7% gain in efficiency. Therefore, the viscosity and thermal conductivity model developed in this paper for high-enthalpy flows represents a balance between efficiency and accuracy across a broad temperature range of $100K$ to $9000K$. It aligns closely with the Yos-Gupta model in terms of accuracy and is an improvement on the Blottner model in non-equilibrium conditions.

The approach presented for modelling the viscosity and thermal conductivity offers a good framework to achieve

computational efficiency and improved accuracy when compared with existing models. The same framework could in principle be used to represent other chemical mixtures or additional flow properties such as diffusion coefficients. For higher temperatures, the influence of ionisation could also be implemented by adding expressions for the contribution from the electronic modes.

Appendix

A. Accuracy and Robustness

Two additional cases for evaluating the present model are demonstrated in this section. First, Fig. 9 shows the transport properties derived using the present model at various constant pressures for equilibrium air over the temperature range of $100K$ to $9000K$. Since the equilibrium composition depends on both pressure and temperature, a change in pressure results in a corresponding change in the equilibrium composition at a given temperature. This case effectively demonstrates the accuracy of the present model in capturing the effect of a chemically non-equilibrium state. The present model produces reasonable results, when compared to the more accurate Yos-Gupta model for high temperatures with negligible differences for temperatures below $5000K$. For turbulence to be present, simulations at higher temperatures than this would normally be associated with pressures above 10^4 Pa [22, 35], where the errors are lower. If necessary, using the same approach presented here, the model coefficients could be re-optimised for extreme pressures..

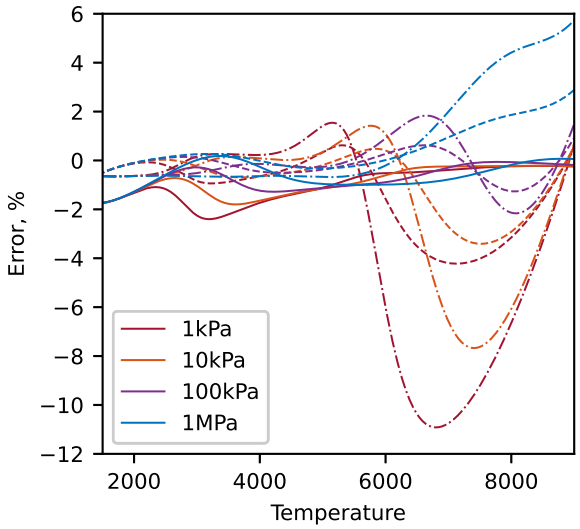

Fig. 9 Relative error of viscosity (solid line), total thermal conductivity (dashed line), and ro-translational thermal conductivity (dashed-dotted line) at different pressures.

Second, to assess the robustness of the present model in chemically non-equilibrium states, a series of 100 random compositions were selected and evaluated across the temperature range of $1000K$ to $9000K$. This was achieved by calculating the properties using both the present model and the Yos-Gupta model, holding the composition constant

across the temperature range, and then statistically deriving the relative mean error as a percentage. This analysis style provides insights into the model's performance in highly chemically non-equilibrium conditions. Figure 10 shows the resulting error.

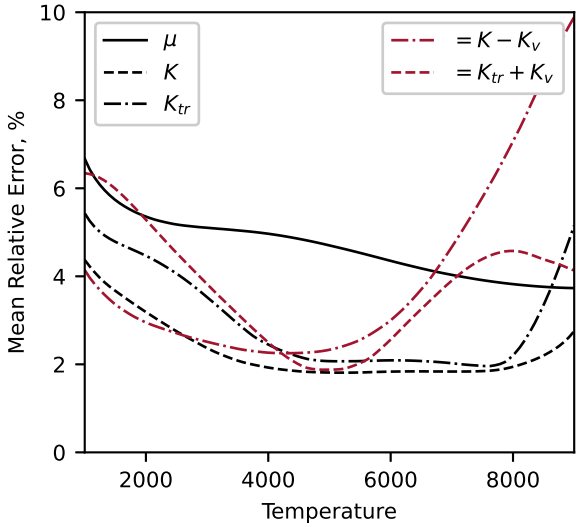

Fig. 10 Evaluation of the robustness of the present model in highly chemical non-equilibrium state.

Acknowledgments

The authors acknowledge the use of the IRIDIS High Performance Computing Facility, and associated support services at the University of Southampton, in the completion of this work.

References

[1] Lee, J. H., "Basic Governing Equations for the Flight Regimes of Aeroassisted Orbital Transfer Vehicles," *19th Thermophysics Conference*, American Institute of Aeronautics and Astronautics Inc. (AIAA), Reston, Virigina, 1984. https://doi.org/10.2514/6.1984-1729.

[2] Gnoffo, P. A., Gupta, R. N., and Shinn, J. L., "Conservation Equations and Physical Models For Hypersonic Air Flows In Thermal and Chemical Nonequilibrium," Tech. Rep. 2867, National Aeronautics and Space Administration (NASA), 1989.

[3] Park, C., "Problems of Rate Chemistry In The Flight Regimes Of Aeroassisted Orbital Transfer Vehicles," *AIAA Paper*, American Institute of Aeronautics and Astronautics Inc. (AIAA), 1984. https://doi.org/10.2514/6.1984-1730.

[4] Park, C., "Review of Chemical-Kinetic Problems of Future NASA Missions, I: Earth Entries," *Journal of Thermophysics and Heat Transfer*, Vol. 7, American Institute of Aeronautics and Astronautics Inc. (AIAA), 1993, pp. 385–398. https://doi.org/10.2514/3.431.

[5] Gupta, R. N., Yos, J. M., Thompson, R. A., and Lee, K.-P., "A Review of Reaction Rates and Thermodynamic and Transport

Properties for an 11-Species Air Model for Chemical and Thermal Nonequilibrium Calculations to 30000 K," Tech. rep., National Aeronautics and Space Administration (NASA), 1990.

[6] Nagnibeda, E., and Kustova, E., *Non-Equilibrium Reacting Gas Flows*, Heat and Mass Transfer, Springer Berlin Heidelberg, Berlin, Heidelberg, 2009. https://doi.org/10.1007/978-3-642-01390-4.

[7] Hirschfelder, J. O., Curtiss, C. F., and Bird, R. B., *Molecular Theory of Gases and Liquids*, John Wiley & Sons Inc, 1954.

[8] Chapman, S., and Cowling, T. G., *The Mathematical Theory of Non-Uniform Gases: An Account of the Kinetic Theory of Viscosity*, Cambridge University Press, 1970.

[9] Yos, J. M., "Transport Properties of Nitrogen, Hydrogen, Oxygen, and Air to 30,000 K," Tech. rep., Massachusetts, 8 1963. URL https://apps.dtic.mil/sti/citations/AD0435053.

[10] Yun, K. S., and Mason, E. A., "Collision Integrals for the Transport Properties of Dissociating Air at High Temperatures," *The Physics of Fluids*, Vol. 5, No. 4, 1962, pp. 380–386. https://doi.org/10.1063/1.1706629.

[11] Yun, K. S., Weissman, S., and Mason, E. A., "High-Temperature Transport Properties of Dissociating Nitrogen and Dissociating Oxygen," *The Physics of Fluids*, Vol. 5, No. 6, 1962, pp. 672–678. https://doi.org/10.1063/1.1706683.

[12] Hao, J., Wang, J., Gao, Z., Jiang, C., and Lee, C., "Comparison of transport properties models for numerical simulations of Mars entry vehicles," *Acta Astronautica*, Vol. 130, 2017, pp. 24–33. https://doi.org/10.1016/J.ACTAASTRO.2016.10.009.

[13] Alkandry, H., Boyd, I. D., and Martin, A., "Comparison of Transport Properties Models for Flowfield Simulations of Ablative Heat Shields," *Journal of Thermophysics and Heat Transfer*, Vol. 28, No. 4, 2014, pp. 569–582. https://doi.org/10.2514/1.T4233.

[14] Tian, Y., Lin, G., and Guo, J., "Analysis of Mass Diffusion Theory and Models for High-Temperature Multi-Component Gases," *International Journal of Heat and Mass Transfer*, Vol. 181, 2021, p. 121994. https://doi.org/10.1016/j.ijheatmasstransfer.2021.121994.

[15] Yos, J. M., "Approximate Equations for the Viscosity and Translational Thermal Conductivity of Gas Mixtures," Tech. rep., Contract Report No. AVSSD-0112-67-RM, Avco Corporation, Wilmington, Massachusetts, 1967.

[16] Gupta, R. N., Lee, K.-P., Thompson, R. A., and Yos, J. M., "Calculations and Curve Fits of Thermodynamic and Transport Properties for Equilibrium Air to 30000 K," Tech. rep., National Aeronautics and Space Administration (NASA), 10 1991.

[17] Wright, M. J., Bose, D., Palmer, G. E., and Levin, E., "Recommended Collision Integrals for Transport Property Computations Part 1: Air Species," *AIAA Journal*, Vol. 43, No. 12, 2005, pp. 2558–2564. https://doi.org/10.2514/1.16713.

[18] Wright, M. J., Hwang, H. H., and Schwenke, D. W., "Recommended Collision Integrals for Transport Property Computations Part II: Mars and Venus Entries," *AIAA Journal*, Vol. 45, No. 1, 2007, pp. 281–288. https://doi.org/10.2514/1.24523.

[19] Palmer, G. E., and Wright, M. J., "Comparison of Methods to Compute High-Temperature Gas Viscosity," *Journal of Thermophysics and Heat Transfer*, Vol. 17, No. 2, 2003, pp. 232–239. https://doi.org/10.2514/2.6756.

[20] Palmer, G., and Wright, M. J., "A Comparison of Methods to Compute High Temperature Gas Thermal Conductivity," *36th AIAA Thermophysics Conference*, 2003. https://doi.org/10.2514/6.2003-3913.

[21] Passiatore, D., Gloerfelt, X., Sciacovelli, L., Pascazio, G., and Cinnella, P., "Direct numerical simulation of subharmonic second-mode breakdown in hypersonic boundary layers with finite-rate chemistry," *International Journal of Heat and Fluid Flow*, Vol. 109, 2024, p. 109505. https://doi.org/10.1016/J.IJHEATFLUIDFLOW.2024.109505.

[22] Passiatore, D., Sciacovelli, L., Cinnella, P., and Pascazio, G., "Shock Impingement on a Transitional Hypersonic High-Enthalpy Boundary Layer," *Physical Review Fluids*, Vol. 8, No. 4, 2023, p. 044601. https://doi.org/10.1103/PhysRevFluids.8.044601.

[23] Passiatore, D., Sciacovelli, L., Cinnella, P., and Pascazio, G., "Thermochemical Non-Equilibrium Effects In Turbulent Hypersonic Boundary Layers," *Journal of Fluid Mechanics*, Vol. 941, 2022, p. A21. https://doi.org/10.1017/jfm.2022.283.

[24] Blottner, F., Johnson, M., and Ellis, M., "Chemically Reacting Viscous Flow Program for Multi-Component Gas Mixtures," Tech. rep., Sandia National Laboratories (SNL), Albuquerque, NM, and Livermore, CA (United States), 12 1971. https://doi.org/10.2172/4658539.

[25] Wilke, C. R., "A Viscosity Equation for Gas Mixtures," *The Journal of Chemical Physics*, Vol. 18, No. 4, 1950, pp. 517–519. https://doi.org/10.1063/1.1747673.

[26] Chen, X. P., Yang, Y. T., and Zhao, S., "Direct Numerical Simulations of High-Enthalpy Supersonic Turbulent Channel Flows Including Finite-Rate Reactions," *Physics of Fluids*, Vol. 36, No. 4, 2024, p. 45153. https://doi.org/10.1063/5.0203414.

[27] Di Renzo, M., and Urzay, J., "Direct Numerical Simulation of A Hypersonic Transitional Boundary Layer At Suborbital Enthalpies," *Journal of Fluid Mechanics*, Vol. 912, 2021, p. A29. https://doi.org/10.1017/jfm.2020.1144.

[28] Khatri, H., and Zhang, L., "Shock Standoff Distance in Viscous Hypersonic Flows around a Blunt Body," AIAA AVIATION 2023 Forum, San Diego, CA and Online, 2023. https://doi.org/10.2514/6.2023-4417.

[29] Zheng, Q., Yang, Y., Wang, J., and Chen, S., "Enstrophy Production and Flow Topology in Compressible Isotropic Turbulence With Vibrational Non-equilibrium," *Journal of Fluid Mechanics*, Vol. 950, 2022, p. A21. https://doi.org/10.1017/jfm.2022.742.

[30] Zheng, Q., Wang, J., Mahbub Alam, M., Noack, B. R., Li, H., and Chen, S., "Transfer of Internal Energy Fluctuation in Compressible Isotropic Turbulence With Vibrational Non-Equilibrium," *Journal of Fluid Mechanics*, Vol. 919, 2021, p. A26. https://doi.org/10.1017/jfm.2021.381.

[31] Margaritis, A. T., Scherding, C., Marxen, O., Schmid, P. J., and Sayadi, T., "Development of a High-Fidelity Computational Tool For Chemically Reacting Hypersonic Flow Simulations," , 10 2022. https://doi.org/https://doi.org/10.48550/arXiv.2210.05547.

[32] Sutherland, W., "The Viscosity of Gases and Molecular Force," *The London, Edinburgh, and Dublin Philosophical Magazine and Journal of Science*, Vol. 36, No. 223, 1893, pp. 507–531. https://doi.org/10.1080/14786449308620508.

[33] Park, C., Jaffe, R. L., and Partridge, H., "Chemical-Kinetic Parameters of Hyperbolic Earth Entry," *Journal of Thermophysics and Heat Transfer*, Vol. 15, No. 1, 2001, pp. 76–90. https://doi.org/10.2514/2.6582.

[34] Millikan, R. C., and White, D. R., "Systematics of Vibrational Relaxation," *The Journal of Chemical Physics*, Vol. 39, No. 12, 1963, pp. 3209–3213. https://doi.org/10.1063/1.1734182.

[35] Volpiani, P. S., "Numerical Strategy To Perform Direct Numerical Simulations of Hypersonic Shock/Boundary-Layer Interaction In Chemical Nonequilibrium," *Shock Waves*, Vol. 31, No. 4, 2021, pp. 361–378. https://doi.org/10.1007/s00193-021-01018-6.

[36] Duan, L., and Martín, M. P., "Direct numerical simulation of hypersonic turbulent boundary layers. Part 4. Effect of high enthalpy," *Journal of Fluid Mechanics*, Vol. 684, 2011, pp. 25–59. https://doi.org/10.1017/JFM.2011.252.

[37] Matyushov, D. V., and Schmid, R., "Calculation of Lennard-Jones Energies of Molecular Fluids," *The Journal of Chemical Physics*, Vol. 104, No. 21, 1996, pp. 8627–8638. https://doi.org/10.1063/1.471551.

[38] Poling, B. E., Prausnitz, J. M., and O'connell, J. P., *Properties of Gases and Liquids*, McGraw-Hill Education, 2001.

[39] Lemmon, E. W., and Jacobsen, R. T., "Viscosity and Thermal Conductivity Equations for Nitrogen, Oxygen, Argon, and Air," *International Journal of Thermophysics*, Vol. 25, No. 1, 2004, pp. 21–69. https://doi.org/10.1023/B:IJOT.0000022327.04529.F3.

[40] Childs, G. E., and Hanley, H. J. M., "The Viscosity and Thermal Conductivity Coefficients of Dilute Nitrogen and Oxygen," Tech. rep., U.S. Government Printing Office, 1966.

[41] Olchowy, G. A., and Sengers, J. V., "A Simplified Representation for the Thermal Conductivity of Fluids in the Critical Region," *International Journal of Thermophysics*, Vol. 10, No. 2, 1989, pp. 417–426. https://doi.org/10.1007/BF01133538/METRICS.

[42] Lemmon, E. W., Jacobsen, R. T., Penoncello, S. G., and Friend, D. G., "Thermodynamic Properties of Air and Mixtures of Nitrogen, Argon, and Oxygen From 60 to 2000 K at Pressures to 2000 MPa," *Journal of Physical and Chemical Reference Data*, Vol. 29, No. 3, 2000, pp. 331–385. https://doi.org/10.1063/1.1285884.

[43] Vincenti, W. G., and Kruger, C. H., *Introduction to Physical Gas Dynamics*, Wiley, New York,, 1965.

[44] Hirschel, E. H., *Basics of Aerothermodynamics*, second, revised ed., Springer International Publishing, 2015. https://doi.org/10.1007/978-3-319-14373-6/COVER.

[45] Vanderslice, J. T., Weissman, S., Mason, E. A., and Fallon, R. J., "High-Temperature Transport Properties of Dissociating Hydrogen," *The Physics of Fluids*, Vol. 5, No. 2, 1962, pp. 155–164. https://doi.org/10.1063/1.1706590.

[46] Mcbride, B. J., Zehe, M. J., and Gordon, S., "NASA Glenn Coefficients for Calculating Thermodynamic Properties of Individual Species," Tech. rep., National Aeronautics and Space Administration (NASA), 2002. URL https://ntrs.nasa.gov/citations/20020085330.

[47] Hilsenrath, J., Benedict, W. S., Fano, L., Hoge, H. J., masa, J. F., Nuttall, R. L., Touloukian, Y. S., and Woolley, H. W., *Tables of Thermal Properties of Gases*, Gaithersburg, MD, 1955. https://doi.org/10.6028/NBS.CIRC.564.

[48] Cengel, Y. A., Boles, M. A., and Kanoglu, M., *Thermodynamics: An Engineering Approach*, McGraw-Hill Education, Singapore, 2019.

[49] Ho, C., and Huerre, P., "Perturbed Free Shear Layers," *Annual Review of Fluid Mechanics*, Vol. 16, No. 1, 1984, pp. 365–422. https://doi.org/10.1146/annurev.fl.16.010184.002053.

[50] Dimotakis, P. E., "Turbulent Free Shear Layer Mixing and Combustion," Tech. rep., California Inst of Tech Pasadena Graduate Aeronautical Labs, 1991. URL https://apps.dtic.mil/sti/citations/ADA243410.

[51] Smits, A. J., and Dussauge, J. P., *Turbulent Shear Layers in Supersonic Flow*, 2nd ed., Springer New York, 2006. https://doi.org/10.1007/B137383.

[52] Lusher, D. J., Sansica, A., Sandham, N. D., Meng, J., Siklósi, B., and Hashimoto, A., "OpenSBLI v3.0: High-Fidelity Multi-Block Transonic Aerofoil CFD Simulations Using Domain Specific Languages on GPUs," *Computer Physics Communications*, Vol. 307, 2025, p. 109406. https://doi.org/10.1016/J.CPC.2024.109406.

[53] Lusher, D. J., Jammy, S. P., and Sandham, N. D., "OpenSBLI: Automated Code-Generation for Heterogeneous Computing Architectures Applied to Compressible Fluid Dynamics on Structured Grids," *Computer Physics Communications*, Vol. 267, 2021, p. 108063. https://doi.org/10.1016/J.CPC.2021.108063.

[54] Chapelier, J. B., Lusher, D. J., Van Noordt, W., Wenzel, C., Gibis, T., Mossier, P., Beck, A., Lodato, G., Brehm, C., Ruggeri, M., Scalo, C., and Sandham, N., "Comparison of High-Order Numerical Methodologies for the Simulation of the Supersonic Taylor-Green Vortex Flow," *Physics of Fluids*, Vol. 36, No. 5, 2024, p. 55146. https://doi.org/10.1063/5.0206359.

[55] Jammy, S. P., Jacobs, C. T., and Sandham, N. D., "Performance Evaluation of Explicit Finite Difference Algorithms with Varying Amounts of Computational and Memory Intensity," *Journal of Computational Science*, Vol. 36, 2019, p. 100565. https://doi.org/10.1016/J.JOCS.2016.10.015.